The Impact of Blade Mounting Structures on Cross-Flow Turbine Performance

Benjamin Strom*[1], Brian Polagye[1], and Noah Johnson[1]

INTRODUCTION

Cross-flow (vertical-axis) turbines have numerous features that make them a promising alternative to axial-flow (horizontal-axis) turbines for marine hydrokinetic applications. First, their normally rectangular form factor makes them ideally suited for the geometry of shallow tidal and river channels. This may also allow for the construction of higher blockage-ratio turbine arrays, potentially boosting array performance [1]. Second, the maximum blade velocity of cross-flow turbines is generally lower than equivalently sized axial-flow devices, reducing the risk of blade cavitation and potential harm to aquatic fauna. Third, cross-flow turbine operation is either bi- or omni-directional, depending on the axis orientation, making them ideally suited for oscillating tidal flows by eliminating the need for active yaw control. Finally, recent work has suggested that optimized arrays of cross-flow turbines may be able to extract more power per area than arrays of axial-flow turbines [2].

In their simplest form, the rotor of a cross-flow turbine consists of a set of blades that rotate about a central axis. Despite this apparent simplicity (just a single degree of freedom), the cyclically varying flow conditions encountered by the blades and the fact that the blades intersect their own wake result in complex hydrodynamics. Studies have been conducted on the effects of various blade geometric parameters, operating conditions, and wake interactions on cross-flow turbine performance. However, little has been published concerning the method of affixing the blades to the central shaft of the turbine. At first glance, this may seem a secondary design parameter in comparison to the rotor blade geometry. However, the blade support structure has the potential to heavily influence rotor performance. First, since the support member(s) must rotate with the rotor, they will necessarily be responsible for some drag opposing the direction of rotation. Second, the support members may influence the lift generation of the rotor blades. On fixed foils, endplates have been shown to act the same as an increase in blade span by reducing tip effects [3]. If of appropriate geometry and placed near the tips of the blades, support spars may perform a similar function. Third, on aircraft wings, winglets are employed to reduce induced drag (drag due to lift)[4]. Foil supports have the potential to play this role. Finally, differing foil support geometries may restrict axial flow in the turbine rotor to varying degrees. This may impact the operation of the turbine rotor when the incoming flow is not perpendicular to the axis of rotation.

Previous studies have individually demonstrated many examples of differing cross-flow turbine geometries, including strategies for mounting the blades to the central shaft. However, to date, few studies have made a systematic comparison. Goude, Lundin, and Leijon [5] considered the influence of the parasitic drag of differing numbers of spars using a double-multiple stream tube model and tabulated values of the spar drag coefficient. Gosselin, Dumas, and Boudreau [6] used an unsteady Reynolds-averaged Naiver-Stokes model to explore the effect of the addition of endplates to a spar-less cross-flow turbine, finding that a small endplate resulted in blade performance gains, due to a reduction in tip-losses, outweighing end-plate drag losses. Li and Calisal [7] experimentally compared a turbine with NACA 0012 struts positioned at the center-span and ends of the blades to a more blunt profile, positioned at 1/4 span from the ends, finding a much lower parasitic drag with the NACA struts. In addition, two types of endplates were tested on the latter turbine resulting in a small increase in performance. Bachant, Wosnik, and Neary [8] compared NACA 0021 cylindrical struts mounted at the mid-span of a three bladed cross-flow turbine via tow-tank experiments. The large drag of the cylindrical struts resulted in a negative turbine efficiency at all tip-speed ratios. Strut drag was measured independently from turbine performance by spinning the turbines without blades.

Cross-flow turbine performance is characterized via the tip-speed ratio (TSR) and rotor mechanical efficiency (C_P) which are given by

$$TSR = \frac{\omega R}{U_\infty} \text{ and } C_P = \frac{\omega \tau}{\frac{1}{2}\rho U_\infty^3 2RH} \quad (1)$$

where ω is the turbine rotation rate, R is the turbine radius, U_∞ is the free stream velocity, τ is the torque produced by the turbine, and H is the turbine height.

EXPERIMENT

Turbine tests were performed in a recirculating water flume with a 75 cm wide and 47 cm deep test section. The turbines measured 17.2 cm in diameter and 23.4 cm high resulting in a blockage ratio of 11.4%. Free stream velocity measurements were made using an acoustic Doppler velocimeter at

*Corresponding Author: strombw@uw.edu

[1]Northwest National Marine Renewable Energy Center, University of Washington, Seattle, WA, USA

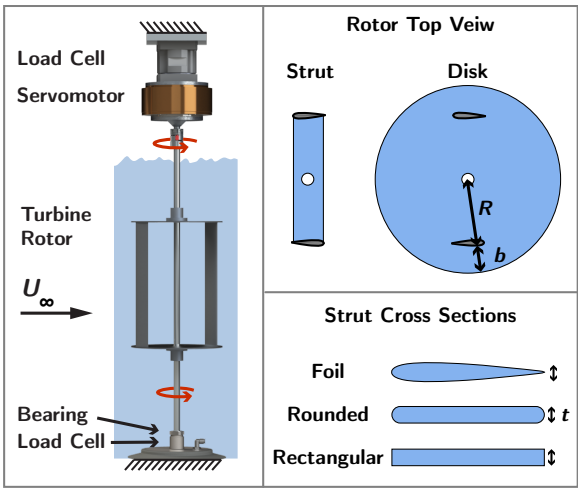

Fig. 1: DIAGRAM OF EXPERIMENTAL SETUP AND STRUT GEOMETRIES. STRUT THICKNESSES TESTED: $t = 0.08c$ and $0.16c$, WHERE c IS THE TURBINE FOIL CHORD. DISK SIZES TESTED: $b = 0, 0.5c$, and, c. NOT SHOWN IS THE "MID-STRUT" (OR "H") CONFIGURATION, WHERE THE BLADES ARE ATTACHED VIA A SINGLE $t = 0.16c$ FOIL AT THE MID-SPAN.

a sample rate of 64 Hz. The turbulence intensity was 1.5% at the maximum flow velocity of 0.7 m/s. The turbine was rotated at a constant angular velocity using a servomotor. Current generated as a result of the servomotor resisting the turbine's rotation was dissipated in a dump resistor. The torque generated by the turbine rotor was measured using a six-axis reaction load cell between the servomotor and a fixed mounting surface. Turbine position was measured using a 2^{18} counts per revolution encoder. The lower end of the turbine shaft was mounted to the flume bottom via a bearing and a second six-axis load cell which gave parasitic bearing torque. Turbine forces and position were sampled at 1000 Hz for a period of 30 seconds for each data point. All tests used two, straight, NACA0015 blades with a chord length of 4.06 cm, resulting in a chord to radius ratio of 0.47 and a solidity (Nc/(pi*D)) of 0.15. The blades were mounted at a preset pitch angle of 6 degrees, leading edge rotated outwards about the quarter chord.

Ten different blade connection geometries were tested. Six types of struts with a chord length equal to the blade chord were tested. These had either a foil, rounded, or rectangular cross-section. For each of these, two thicknesses were tested, 0.16c and 0.08c, as expressed as a fraction of the turbine foil chord length. Additionally, three sets of circular disks were tested. The first had a radius equal to that of the turbine. The second and third had radii that were expanded by 0.5 and 1.0 chord lengths. All spars and disks were mounted to the ends of the turbine blades with the exception of a final "mid-strut" configuration, in which the blades were mounted to the center shaft at the mid-span using a 0.16c thick foil. Turbine geometries are further detailed in figure 1.

By incrementing the tip-speed ratio, a complete performance curve was generated for each spar geometry for four different free stream velocities. These corresponded to blade chord Reynolds numbers of 18.2, 22.8, 27.4 and 31.8 $\times 10^3$. Additionally, parasitic spar losses were estimated by performing the same tip-speed ratio sweep without turbine blades at the highest Reynolds number.

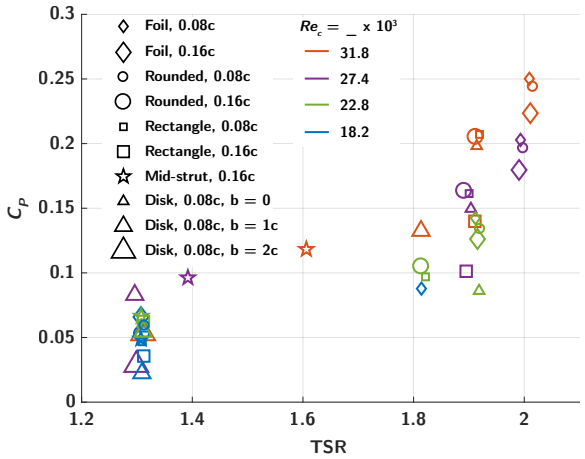

Fig. 2: PEAK TURBINE EFFICIENCY AS A FUNCTION OF CORRESPONDING TSR. COLOR INDICATES REYNOLDS NUMBER (cU_∞/ν). LEGEND INDICATES STRUT SHAPE AND THICKNESS.

RESULTS

Figure 2 summarizes the results by showing peak performance of each turbine geometry as a function of Reynolds number and tip-speed ratio. Without exception, increasing Reynolds number increased turbine performance. For poor-performing turbines, a secondary performance curve peak at TSR = 1.3 dominates over the peak near TSR = 1.8-2. Previous work has demonstrated that this low-TSR peak is due to a strong vortex-foil interaction. Increasing turbine performance generally corresponds to an increase in TSR at peak efficiency. At the highest Reynolds number, strut geometries with the greatest peak efficiencies were the 0.08c thick struts with foil and rounded cross sections ($C_P = 0.250$ and 0.244, respectively) followed by the 0.16c thick strut with a foil cross section ($C_P = 0.224$). At the highest Reynolds number, the smallest disk ($b = 0$), thin rectangular strut, and thick rounded strut performed similarly.

DISCUSSION

Taking a perturbation theory-like approach to the problem, the total efficiency of the turbine can be broken up as follows

$$C_{P,\,\text{total}} = C_{P,\,\text{blades}} + C_{P,\,\text{spars}} + C_{P,\,\text{s}\to\text{b}} + C_{P,\,\text{b}\to\text{s}} + C_{P,\,\text{h.o.t.s}} \tag{2}$$

Here $C_{P,\,\text{blades}}$ represents the power produced by the blades, regardless of the mounting geometry. $C_{P,\,\text{spars}}$ represents the parasitic losses due to drag on the spars. The next two terms represent higher-order, secondary effects. $C_{P,\,\text{s}\to\text{b}}$ represents the influence the presence of the spars has on blade performance. This includes the end-plate effect, reduction of induced drag, and influence on axial flow. $C_{P,\,\text{b}\to\text{s}}$ represents the influence the presence of the blades has on the drag on the spars, primarily changes in the flow field due to the turbine blades. Further, higher order effects ($C_{P,\,\text{h.o.t.s}}$) likely exist, but are not considered in this analysis.

The importance of secondary effects can be explored by first assuming they are small enough to be ignored. If this is true, then

$$C_{P,\,\text{blades}} = C_{P,\,\text{total}} - C_{P,\,\text{spars}} - C_{P,\,\text{secondary}}. \tag{3}$$

As in [8], measurements of $C_{P,\,\text{spars}}$ have been taken directly by spinning the turbine in the flume without blades. If the

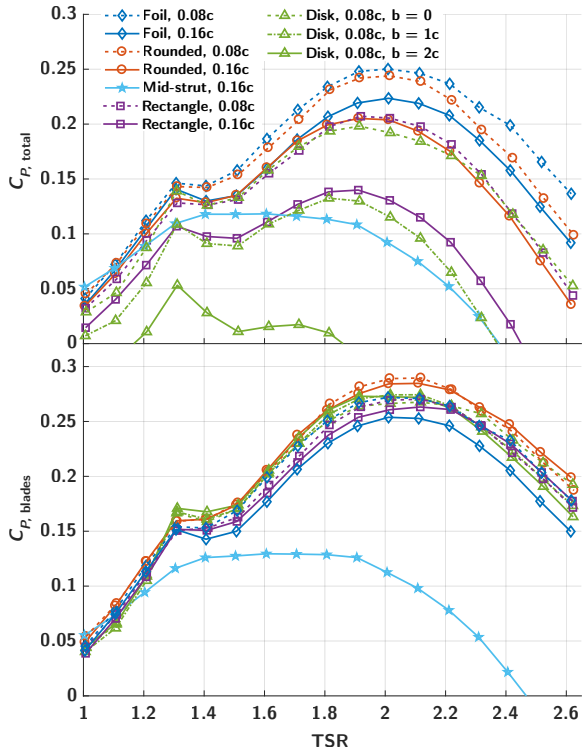

Fig. 3: PERFORMANCE CURVES WITHOUT (TOP) AND WITH (BOTTOM) PARASITIC STRUT DRAG REMOVED AT REYNOLDS NUMBER 31.8×10^3.

approximation that $C_{P,\,\text{secondary}} \approx 0$ holds, $C_{P,\,\text{blades}}$ should then be the same for all turbine configurations. Figure 3 shows the performance curves resulting from this analysis. Though the curves are greatly collapsed, secondary effects are still responsible for significant performance variation. At the peak of the curve there is a 13% difference in the lowest and highest performing geometries. This discrepancy increases with TSR. Since the largest variation is between turbines with identical planform geometries (Foil, 0.16c versus Rounded 0.08c), it is hypothesized that the most influential secondary effect is $C_{P,\,\text{b}\to\text{s}}$, or the influence of the presence of the blades on the drag on the spars. Extending the disk spars beyond the radius of the turbine foils did not appear to increase blade performance. This suggests that shielding the inside edge of the blade (suction side) only is adequate to reduce tip losses. Since the mid-strut turbine is the only geometry with free foil tips, it is likely that $C_{P,\,\text{s}\to\text{b}}$ dominates, as flow is no longer blocked from the blade suction surface to the opposite side, and top-losses are large. This explains the poor total and blade performance of the mid-strut turbine (star symbols in Fig. 2).

Modeling Strut Drag

Analytical models for the drag on various spar geometries may be a useful design tool. First the rectangular-planform (non-disk) spars are considered. The relative velocity perpendicular to a strut section a distance r from the rotation axis may be written as

$$U_{\text{rel}} = \omega r + U_\infty \cos(\theta) + U_{\text{induced}} \tag{4}$$

where θ is the blade position and is zero when the blade is traveling directly upstream. U_{induced} consists of any flow velocities induced by the turbine and spars. This term will be neglected in subsequent analysis. The torque due to drag on a spar element of width dr is

$$\tau_d(r,\theta) = \frac{1}{2}\rho U_{\text{rel}}(r,\theta)^2\ \text{sgn}(U_{\text{rel}}) C_D(U_{\text{rel}}) L dr. \tag{5}$$

Here L is the characteristic length used in the drag coefficient (C_D) definition. The $\text{sgn}(U_{\text{rel}})$ term ensures the torque is applied in the direction of the relative velocity in case reverse flow is encountered. The power lost to N struts is then given by

$$P_{\text{strut}} = \frac{\omega N \rho L}{2\pi} \int_0^{2\pi}\int_0^R U_{\text{rel}}(r,\theta)^2\ \text{sgn}(U_{\text{rel}}) C_D(r,\theta)\,(U_{\text{rel}})\, r dr d\theta. \tag{6}$$

First we will consider the rectangular and rounded struts. Here $L = t$, the strut thickness. Because the variation in drag coefficient with Reynolds number has been shown to be small [9], a constant value is used. A good approximation is to neglect the effect of reverse flow, since it occurs for only a small portion of the rotation, and if the TSR is greater than 1, only near the center of the turbine where U_{rel} is small. Then the power loss can be solved exactly as

$$P_{\text{rect.}} = \frac{1}{4}\omega N \rho C_D t R^2 \left(\omega^2 R^2 + U_\infty^2\right). \tag{7}$$

Drag coefficients of 0.95 and 0.92 where found to best fit the $0.16c$ and $0.08c$ rectangular struts respectively.

Equation (6) is modified to simulate the foil strut power loss by allowing the drag coefficient to vary based on the instantaneous Reynolds number (via table look-up) and changing the characteristic length to the chord ($L = c$).

$$P_{\text{foil strut}} = \frac{\omega N \rho c}{4\pi} \int_0^{2\pi}\int_0^R U_{\text{rel}}(r,\theta)^2\ \text{sgn}(U_{\text{rel}}) C_D(r,\theta) r dr \tag{8}$$

Modeling Disk Drag

Von Karman [10] solved the the Navier Stokes Equations for the flow over a rotating disk, with improvements made by Cochran [11]. Rott and Lewellen [12] extended the approach to include the translation of the disk. For this solution, the drag torque on the disk is the same with or without translation (free-stream flow). This is because the effects on the boundary layer of the free-stream flow cancel on advancing and retreating sides of the disk. Neglecting the effects of the edge and of reverse flow, the total drag torque on one side of the disk was found via numerical integration [12] to be

$$\tau_{\text{disk}} = -\frac{1}{2}\pi G'(0) \rho R^{*4} \sqrt{\nu \omega^3}. \tag{9}$$

The parasitic drag power loss for the disk geometry is then

$$P_{\text{disks}} = 4\tau_{\text{disk}}\omega = -2\pi G'(0) \rho R^{*4} \sqrt{\nu \omega^5}, \tag{10}$$

where $R^* = R + b$ is the disk radius, ν is the kinematic viscosity, ρ is the fluid density, and $G'(0)$ is a constant resulting from the numeric integration [11], [10] . The data collected in this experiment suggest that the power loss to the disks is not completely independent of the free-stream velocity, as is the case in this laminar flow solution. This may be due to a boundary layer which becomes turbulent over some portion of the disk. This is especially likely downstream of the support shaft where the shaft wake may trip the boundary layer transition. In addition, turbulence in the free-stream flow may result in a premature turbulent boundary layer. A successful modification is to replace $G'(0)$ with $c_1 U_\infty^{c_2}$, where constants c_1 and c_2 are chosen to best fit all data collected, resulting in

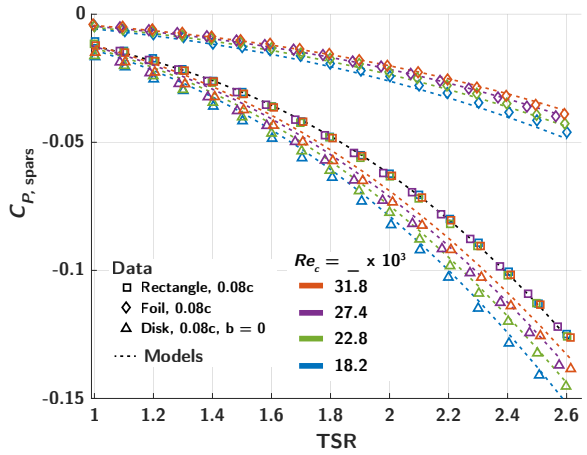

Fig. 4: EFFICIENCY LOSS DUE TO STRUT DRAG VERSUS TSR DATA (SYMBOLS) COMPARED TO MODELS (LINES) GIVEN BY EQUATIONS (7), (8), AND (11).

$c_1 = 1.435$ and $c_2 = 0.256$. These constant values have good agreement of the range of tip-speed ratios, disk radii, and free stream velocities tested. This yields in a power loss of

$$P_{\text{disks}} = -2\pi c_1 U_\infty^{c_2} \rho R^{*4} \sqrt{\nu \omega^5} \tag{11}$$

for the two-disk system.

Note that though these experiments were conducted using a turbine with just two blades, the models for power loss given here may be used to select the optimal blade attachment method depending on the number of blades. For example, while the thin foil strut is shown here to be optimal for a two-bladed turbine, the addition of blades will increase power lost to drag on additional struts, while the losses due to a disk spar will not change. Extrapolation of the data here shows that a six-bladed turbine should perform equally well using the $b = 0$ disk or thin foil struts.

Fig. 4 shows a comparison of the three models presented here with measurements of spar efficiency loss, made by spinning the spars without blades. Reasonable agreement is found, including Reynolds number dependence of the disk and foil spars.

CONCLUSIONS

Ten cross-flow turbine foil mounting geometries have been tested at four Reynolds numbers. The best-performing mounting system consists of thin foil-shaped struts attached at the ends of the turbine blades. Except the mid-strut design, correcting for losses due to strut drag, blade performance was shown to collapse to within a range of $\Delta C_P = 0.04$ at peak performance. Models for strut power loss are shown to match well with data and may be useful as design tools. Ongoing and future work includes analysis of the impact of Reynolds number and off-axis flow on turbine performance and optimal spar design. Additional spar geometries such as foil struts which incorporate small end-plates or winglets and a curved foil-strut interface are under consideration.

ACKNOWLEDGMENT

We would like to thank Naval Facilities Engineering Command for funding this research.

REFERENCES

[1] Salter, S., 2012. "Are nearly all tidal stream turbine designs wrong?". In 4th International Conference on Ocean Energy.

[2] Dabiri, J. O., 2011. "Potential order-of-magnitude enhancement of wind farm power density via counter-rotating vertical-axis wind turbine arrays". *Journal of Renewable and Sustainable Energy,* ***3***(4), p. 043104.

[3] Reid, E., 1924. "The effects of shielding the tips of airfoils", naca rep. 201". *Natl. Advis. Comm. Aeronaut., Hampton, VA*.

[4] Kroo, I., 2001. "Drag due to lift: concepts for prediction and reduction". *Annual Review of Fluid Mechanics,* ***33***(1), pp. 587–617.

[5] Goude, A., Lundin, S., and Leijon, M., 2009. "A parameter study of the influence of struts on the performance of a vertical-axis marine current turbine". In Proceedings of the 8th European wave and tidal energy conference, EWTEC09, Uppsala, Sweden, Citeseer, pp. 477–483.

[6] Gosselin, R., Dumas, G., and Boudreau, M., 2013. "Parametric study of h-darrieus vertical-axis turbines using urans simulations". *21st Annual Conference of the CFD Society of Canada*.

[7] Li, Y., and Calisal, S. M., 2010. "Three-dimensional effects and arm effects on modeling a vertical axis tidal current turbine". *Renewable energy,* ***35***(10), pp. 2325–2334.

[8] Bachant, P., Wosnik, M., Gunawan, B., and Neary, V. S., 2016. "Experimental study of a reference model vertical-axis cross-flow turbine". *PloS one,* ***11***(9), p. e0163799.

[9] Schewe, G., 2013. "Reynolds-number-effects in flow around a rectangular cylinder with aspect ratio 1: 5". *Journal of Fluids and Structures,* ***39***, pp. 15–26.

[10] Kármán, T. V., 1921. "Über laminare und turbulente reibung". *ZAMM - Journal of Applied Mathematics and Mechanics / Zeitschrift für Angewandte Mathematik und Mechanik,* ***1***(4), pp. 233–252.

[11] Cochran, W., 1934. "The flow due to a rotating disc". In Mathematical Proceedings of the Cambridge Philosophical Society, Vol. 30, Cambridge Univ Press, pp. 365–375.

[12] Rott, N., and Lewellen, W. S., 1967. "Boundary layers due to the combined effects of rotation and translation". *The Physics of Fluids,* ***10***(9), pp. 1867–1873.